Field-induced phase transitions and phase diagrams in $BiFeO_3$-like multiferroics

Z. V. Gareeva,[1,2,*] A. F. Popkov,[3] S. V. Soloviov,[3] and A. K. Zvezdin[4,5,6]

[1]*Institute of Molecular and Crystal Physics, Russian Academy of Sciences, 450075, Ufa, Russia*

[2]*Bashkir State University, 450076, Ufa, Russia*

[3]*National Research University of Electronic Technology, 124498, Zelenograd, Moscow, Russia*

[4]*A.M. Prokhorov General Physics Institute, Russian Academy of Sciences, 119991, Moscow, Russia*

[5]*P.N. Lebedev Physical Institute of the Russian Academy of Sciences, 119991, Moscow, Russia*

[6]*Moscow Institute of Physics and Technology (State University), 141700, Dolgoprudny, Russia*

(Received 18 February 2013; revised manuscript received 7 April 2013; published xxxxx)

We explore incommensurate magnetic structures and phase diagrams of multiferroics through accurate micromagnetic analysis, taking into account the spin flexoelectric interaction (the so-called Lifshitz invariant). We consider $BiFeO_3$ single crystals and epitaxial films grown on (111) substrates. The main control parameters of these systems are the magnetic field, magnetic anisotropy, and, in the case of thin films, epitaxial strain. We construct phase diagrams representing stability regions for the homogeneous magnetic states and incommensurate structures for two geometries of the field (parallel to the principal crystal axis $\boldsymbol{H}\|\boldsymbol{C}_3$ and perpendicular to this direction $\boldsymbol{H}\perp\boldsymbol{C}_3$). It is shown that the direction of applied magnetic field substantially affects the magnetic phases, the properties of incommensurate structures, and the character of phase transitions. A conical type of cycloidal ordering is revealed to exist during the transition from the incommensurate cycloidal structure to the homogeneous magnetic state. Constructed phase diagrams provide the combination of control parameters required to suppress the cycloidal ordering. Our results show that the critical magnetic field for suppression of the cycloid is lower in thin films than in single crystals, and can also be lowered by appropriate selection of applied magnetic field orientation. These results provide a stronger understanding of the complex magnetic ordering in $BiFeO_3$ and can be useful for strain engineering of new multiferroic materials on demand.

DOI: 10.1103/PhysRevB.00.004400 PACS number(s): 75.85.+t, 75.50.Ee, 75.30.Kz, 75.30.Fv

I. INTRODUCTION

Multiferroic materials are compounds that have coupled magnetic, ferroelectric, and ferroelastic orders. The interest in these materials is driven by the prospect to control charges by applied magnetic fields and spins by applied voltages. They have potential applications in nanoelectronics, sensors, photovoltaics, and energy harvesting.[1–8]

Although the number of multiferroic materials increases the one of the most studied multiferroics remains bismuth ferrite ($BiFeO_3$ or BFO). BFO has extraordinary ferroelectric[1,2,9] and unexpected transport properties.[10,11] It has been used as a blocking layer in spin valves[12,13] to control their giant magnetoresistance (GMR) by an electric field and also as a gate dielectric layer in magnetoelectric field effect devices.[14] BFO can be interesting for magnonics[15] since their magnon spectra can be electrically controlled over a wide range.[16]

The structure and properties of BFO bulk single crystals have been extensively studied.[9,17–19] BFO has high temperatures of ferroelectric $T_C = 1083$K and antiferromagnetic ordering $T_N = 643$K, an electric polarization of the order 1 C/m^2 and magnetization of the order 5 emu/cm^3.[2,7,20] Its crystal structure is based on ABO_3 perovskite structure. Three types of distortions: relative displacement of Bi and Fe ions along $\langle 111\rangle$ axis, deformations of oxygen octhahedral, and counterrotation of oxygen octhahedral around the $\langle 111\rangle$ axis reduce the perovskite symmetry group to the $R3c$ space group. The spontaneous polarization, caused by the distortions, appears along one of the eight pseudocubic $\langle 111\rangle$ directions.

The magnetic structure of BFO in the first approximation is G-type antiferromagnetic, with weak ferromagnetic component, as established by Kiselev *et al.*[21] Further neutron diffraction studies[22–24] showed that the G-type antiferromagnetic structure is superimposed with a cycloidal modulation with period 62 nm (Fig. 1). Since in the bulk eight directions of polarization are allowed, several directions of the cycloid propagation are possible. Although there is the possibility that the cycloid be either left- or right- handed, cycloids observed in the bulk were found to be of single chirality.[22] According to Ref. 25 the cycloidal magnetic structure exists below 650 K on cooling down to critical temperature of 4 K. The explanation of the complicated spin arrangement in BFO requires taking into account specific spin flexoelectric (or flexomagnetoelectric) interaction.

The corresponding additional term arising in a free energy expansion in crystals of $R3c$ symmetry group is known as the Lifshitz invariant. In Ref. 26 it was shown that the presence of the Lifshitz invariant leads to a solution related to cycloidal spin arrangement. The relationship between the Lifshitz invariant and the related Dzyaloshinskii-Morya interaction was discussed in Ref. 27.

The first observations of space-modulated structures refer to metallic magnets; later on the spiral magnetic ordering was discovered in magnetic dielectrics (antiferromagnets), particularly BFO. At present many multiferroics with helical magnetic ordering are known.[28,29] The theoretical description of incommensurate superstructures in ferromagnetic metals was elaborated by Dzyaloshinskii.[30] Within the same approach the cycloidal magnetic ordering in BFO was explained taking into account the mechanism of inhomogeneous magnetoelectric interactions.[30–35] The spin cycloid at room temperatures is well described by harmonic functions $\sin(\boldsymbol{k}\cdot\boldsymbol{r})$, $\cos(\boldsymbol{k}\cdot\boldsymbol{r})$, where $\boldsymbol{k}$ is the wave vector of spin propagation. In the

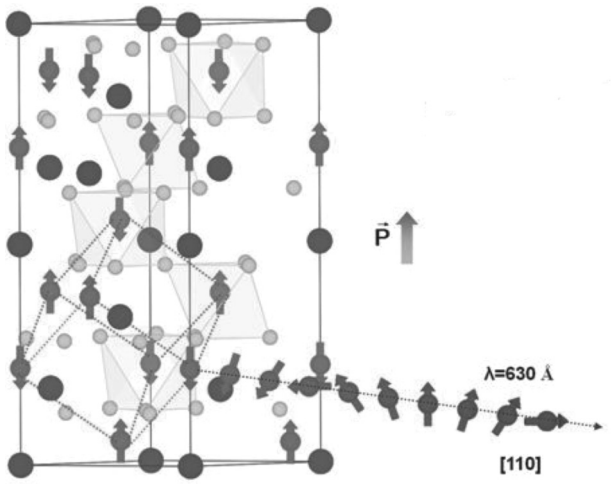

FIG. 1. BFO unit cell, schematic illustration of spin cycloid.

general case, the spin distribution in the cycloid obeys an anharmonical law and is described with the Jacobi elliptical functions $sn(\boldsymbol{k}\cdot\boldsymbol{r};\nu)$, $cn(\boldsymbol{k}\cdot\boldsymbol{r};\nu)$ where ν defines the degree of anharmonicity. A change of temperature,[25] rare-earth ion doping,[36–38] magnetic and electric fields,[39–41] and stresses induced by orienting substrate[42–45] are external factors that can affect the parameter ν. Slight structural modifications in BFO thin film can cause drastic changes in the magnetic structure.[42] A broad array of magnetic phases can be realized in BFO films depending on the type of substrate, crystallographic orientation of the film, chemical doping, or presence of ferroelectric domain structure.[36–38,42–46]

The aim of this work is to analyze the possible commensurate and incommensurate magnetic structures that can be realized in single BFO crystals and in (111)-oriented films, as well as the investigation of the transitions between modulated and homogeneous magnetic states under external conditions. In our treatment, magnetic field and magnetic anisotropy are taken as the key parameters regulating the appearance of the magnetic phases and their restructuring processes. We argue that micromagnetic structure is modified under temperature variations of exchange and induced anisotropy parameters, and that the magnetic field is an important factor controlling magnetic states. Our findings show that incommensurate magnetic phase is complex, and that it comprises different phases between which phase transitions occur when parameters of the system are changed. Presently, the incommensurate phase in BFO multiferroics is considered a cycloidal structure where spins rotate in the plane passing through the principal crystal axis and one of the axes lying in a crystal basal plane. We show, however, that new cycloidal phases with three-dimensional spin reorientation arise with the change of external magnetic field and magnetic anisotropy. The most essential geometries of magnetic field (magnetic field oriented along principal crystal axis $\boldsymbol{C}_3$ and in the direction perpendicular to $\boldsymbol{C}_3$) have been considered, and phase diagrams in terms of magnetic field and magnetic anisotropy have been constructed.

The paper is organized as follows. Section II discusses the problem and presents the theoretical model and governing equations. Section III treats homogeneous magnetic states, incommensurate states and phase diagrams of BFO multiferroics in the magnetic field applied along the principal axis $\boldsymbol{H}\|\boldsymbol{C}_3$. Sections IV and V present a similar analysis for the case of the magnetic field applied in the basal plane of the film. We concentrate on limiting situations concerning the magnetic field oriented along the direction of cycloid space modulation $\boldsymbol{H}\|\boldsymbol{OX}\|[1\bar{1}0]$ (Sec. IV) and magnetic field oriented in the perpendicular direction $\boldsymbol{H}\|\boldsymbol{OY}\|[11\bar{2}]$ (Sec. V); the phase diagram related to the situation $\boldsymbol{H}\perp\boldsymbol{C}_3$ is presented in Sec. V.

Experiments have shown that the cycloid is suppressed by high magnetic fields[39–41] and is not always observed in BFO thin films.[47] The phase diagram of the stability of the magnetic states presented in this paper will enable estimation of conditions that define the type of space-modulated structures that exist, and furthermore, the conditions required for the destruction of the space-modulated state.

II. GENERAL EQUATIONS

In this section the formalism of the micromagnetism approach is developed to describe magnetic phases in BFO multiferroics considered both in a single crystal and in films. The symmetry and crystallographic structure of the film differ from those of single crystal and consequently crystals and films can possess different physical properties. BFO is a strong example of this assessment. It is known that BFO films can demonstrate semiconducting properties or even become metallic in specific conditions while BFO single crystals are known as insulators. However, in our consideration we investigate the magnetic properties of BFO films, while limiting the problem with a range of parameters, which do not allow strong structural changes. (111)-oriented BFO film with rhombohedral crystallographic structure the same as BFO crystal is considered.

The determination of magnetic structures and the construction of corresponding phase diagrams is based on the known variational problem of free energy functional minimization, namely $\delta\Phi = \delta\int F dV = 0$ with the condition $\delta^2\Phi > 0$.

The free energy density of a BFO-like crystal is represented in the form

$$F = F_{\lambda D} + F_{ex} + F_{an} + F_L + F_H + F_{m.\mathrm{elas}}, \qquad (1)$$

where

$$F_{\lambda D} = \lambda \boldsymbol{M}_1\cdot\boldsymbol{M}_2 + \boldsymbol{D}[\boldsymbol{M}_1\times\boldsymbol{M}_2] \qquad (2)$$

is the isotropic and the Dzyaloshinskii-Morya exchange interaction energy density, $\boldsymbol{M}_1$ and $\boldsymbol{M}_2$ are the sublattice magnetizations, λ is the antiferromagnetic exchange coupling parameter, $\boldsymbol{D} = D\boldsymbol{n_c}$ is the Dzyaloshinskii vector, $\boldsymbol{n_c}$ is the unit vector oriented along crystal principal axis, and D is the Dzyaloshinskii parameter. In antiferromagnetism theory it is accepted to use ferromagnetic and antiferromagnetic order parameters $\boldsymbol{M} = \boldsymbol{M}_1 + \boldsymbol{M}_2$, $\boldsymbol{L} = \boldsymbol{M}_1 - \boldsymbol{M}_2$ or dimensionless variables $\boldsymbol{m} = \boldsymbol{M}/2M_0$, $\boldsymbol{l} = \boldsymbol{L}/2M_0$.

In terms of $\boldsymbol{M},\boldsymbol{L}$ the Dzyaloshinskii-Morya exchange interaction energy density can be rewritten in the form

$$F_{\lambda D} = \frac{\lambda}{4}(\boldsymbol{M}^2 - \boldsymbol{L}^2) + \frac{D}{2}\boldsymbol{M}[\boldsymbol{n_c}\times\boldsymbol{L}]. \qquad (3)$$

The exchange energy density acquires a form

$$F_{ex} = A \sum_{x,y,z} (\nabla l_i)^2, \tag{4}$$

where A is the stiffness constant l_i, $i = x,y,z$ are the components of the unit antiferromagnetic vector $\boldsymbol{l}$, and M_0 is the sublattice magnetization. The nonuniform magnetoelectric interaction energy density, known as the Lifshitz invariant, is written as

$$F_L = \beta(l_x \nabla_x l_z + l_y \nabla_y l_z - l_z \nabla_x l_x - l_z \nabla_y l_y), \tag{5}$$

where $\boldsymbol{OX} \| [1\bar{1}0]$, $\boldsymbol{OY} \| [11\bar{2}]$, $\boldsymbol{OZ} \| [111]$, the spontaneous electric polarization vector $\boldsymbol{P}$ is assumed to be oriented along [111], β is the constant of the nonuniform magnetoelectric interaction, with its sign dependent in particular on the orientation of vector $\boldsymbol{P}$. For the definiteness we suppose below that $\beta > 0$; in the case of BFO multiferroics $\beta \approx 0.6$ erg/cm^2.

The Zeeman energy density is given by

$$F_H = -\boldsymbol{M} \cdot \boldsymbol{H}, \tag{6}$$

where $\boldsymbol{H}$ is the applied magnetic field; the magnetic anisotropy energy density is represented as

$$F_{an} = -K_u l_z^2, \tag{7}$$

where K_u is the constant of uniaxial magnetic anisotropy.

The effective magnetic anisotropy in films can be different from the one in single crystals. It is shown below that in the case of (111)-oriented BFO films, uniaxial magnetic anisotropy has an additional contribution related to the magnetoelastic energy density

$$F_{m.\text{elas.}} = -\frac{B_2 u_0}{2} l_z^2, \tag{8}$$

where B_2 is the magnetoelastic constant, u_0 is the mismatch parameter determined over film and substrate lattice parameters a_{film}, a_{subs}

$$u_0 = \frac{a_{\text{subs}} - a_{\text{film}}}{a_{\text{film}}}. \tag{9}$$

The lattice mismatch depends on their values in a single crystal, the growth conditions of the heterostructure, temperature, and thickness of the film.[48,49] As seen from (7), (8) consideration of the magnetoelastic interaction leads to the renormalization of the uniaxial magnetic anisotropy constant $\widetilde{K_u} = K_u + B_2 u_0/2$.

At low temperatures $T \ll T_N$ (T_N is the Neel temperature) ferromagnetic and antiferromagnetic vectors satisfy the relations

$$\begin{aligned} \boldsymbol{l}^2 + \boldsymbol{m}^2 &= 1 \\ \boldsymbol{l} \cdot \boldsymbol{m} &= 0. \end{aligned} \tag{10}$$

In relatively weak magnetic fields $H \ll H_{ex}$ ($H_{ex} \approx 10^7$Oe in BFO) these additional conditions allow the exclusion of the vector $\boldsymbol{m}$ from the minimization problem, and the free energy density F can be represented in terms of the unit vector $\boldsymbol{l}$ and its derivatives.

$$F = -\frac{\chi_\perp}{2}\left(\boldsymbol{H}_{\text{eff}}^2 - (\boldsymbol{H}_{\text{eff}} \cdot \boldsymbol{l})^2\right) + F_{ex} + F_{an} + F_L + F_{m.\text{elas}}, \tag{11}$$

where $\boldsymbol{H}_{\text{eff}} = M_0 \boldsymbol{h} + D[\boldsymbol{l} \times \boldsymbol{e_p}]$, $\boldsymbol{e_p} = (0,0,1)$ is the unit vector of spontaneous polarization $\boldsymbol{P}$ oriented along the principal crystal axis, $\boldsymbol{h} = \boldsymbol{H}/M_0$.

Hereinafter we transform to the reduced parameters $\kappa_c, \kappa_m, \kappa_d$ determined as

$$\begin{aligned} \kappa_c &= \frac{4A}{\beta^2}\left(-\widetilde{K_u} + \frac{\chi_\perp H_D^2}{2}\right) \\ \kappa_m &= \chi_\perp M_0^2 \frac{2A}{\beta^2} \\ \kappa_d &= \chi_\perp H_D^2 \frac{2A}{\beta^2}, \end{aligned}$$

where $H_D = D$ is the Dzyaloshinskii field, and $\chi_\perp$ is the transversal magnetic susceptibility of the antiferromagnet.

In the calculations carried out below we have chosen parameter values characteristic of the multiferroics BFO. Literature values of the exchange stiffness A are in the range of $(2-4) \times 10^{-7}$erg/cm.[9,26,50] Below we have taken $A = 3 \times 10^{-7}$erg/cm. The magnetization M_0 on various estimates[2,7,20,51] is in the range $(2-5)$ emu/cm^3 (films doped by rare-earth ions have larger values of magnetization), we put $M_0 = 5$ emu/cm^3. The Dzyaloshinskii-Moriya interaction field, estimated from measurements of electron paramagnetic resonance,[52] is $H_d = 1.2 \times 10^5$Oe. Transverse susceptibility of an antiferromagnet by Ref. 53 equals $\chi_\perp = 4 \times 10^{-5}$. Magnetostriction and magnetic anisotropy of the perovskitelike antiferromagnets varies rather widely.[50,54,55] If we assume that the variation of the induced anisotropy in BFO is in the range 10^4erg/cm^3 $< |\widetilde{K_u}| < 10^6$erg/cm^3, then it corresponds to a change of the normalized parameter κ_c in the range $-5 < |\kappa_c| < 5$.

The reduced free energy density $E = 2AF/\beta^2$ in terms of the variables κ_c, κ_d, κ_m, $\widetilde{x} = x\beta/2A$ acquires the form

$$\begin{aligned} E = \frac{1}{2}\Bigg[&\left(\frac{\partial l_x}{\partial \widetilde{x}}\right)^2 + \left(\frac{\partial l_y}{\partial \widetilde{x}}\right)^2 + \left(\frac{\partial l_z}{\partial \widetilde{x}}\right)^2 + \left(\frac{\partial l_x}{\partial \widetilde{y}}\right)^2 + \left(\frac{\partial l_y}{\partial \widetilde{y}}\right)^2 + \left(\frac{\partial l_z}{\partial \widetilde{y}}\right)^2\Bigg] \\ &+ \left(l_x \frac{\partial(\boldsymbol{l} \cdot \boldsymbol{e_p})}{\partial \widetilde{x}} + l_y \frac{\partial(\boldsymbol{l} \cdot \boldsymbol{e_p})}{\partial \widetilde{y}} - (\boldsymbol{l} \cdot \boldsymbol{e_p})\frac{\partial l_x}{\partial \widetilde{x}} - (\boldsymbol{l} \cdot \boldsymbol{e_p})\frac{\partial l_y}{\partial \widetilde{y}}\right) + \frac{1}{2}\kappa_c l_z^2 + \frac{1}{2}\kappa_m (\boldsymbol{h} \cdot \boldsymbol{l})^2 - \sqrt{\kappa_m \kappa_d}\boldsymbol{h}[\boldsymbol{e_p} \times \boldsymbol{l}]. \end{aligned} \tag{12}$$

Due to the identity $|\boldsymbol{l}^2| = 1$ the vector $\boldsymbol{l}$ may be determined by the two coordinates $q_i = \theta,\varphi$ $(i = 1,2)$, which are the polar and the azimuthal angles in spherical coordinate frame. The polar angle is measured from the equilibrium position of antiferromagnetic vector $\boldsymbol{l}_0$, the azimuthal angle is measured from its projection on the orthogonal plane.

In this paper we restrict ourselves to the investigation of one-dimensional magnetic structures depending on the x coordinate. In this assumption the equation $\delta\Phi = 0$ results in the Euler-Lagrange equation

$$-\frac{\partial}{\partial x}\frac{\partial F}{\partial q_i'} + \frac{\partial F}{\partial q_i} = 0, \tag{13}$$

where $q_i' = \partial q_i/\partial x$, $i = 1,2$.

Let $q_{0\alpha}(x)$ be a set of magnetic structures determined by Eq. (13) where α enumerates a set of solutions of Eq. (13) ($\alpha = 1,2,3,\ldots$). The condition of stability $\delta^2\Phi > 0$ of magnetic structure $q_{0\alpha}$ arrives at the Sturm-Liouville eigenvalue problem

$$\widehat{L}_{ij}(q_{0\alpha})\delta q_{\alpha j} = \rho_{\alpha i}\lambda_\alpha \delta q_{\alpha i}, \tag{14}$$

where the functions $\delta q_{\alpha i} = q_i - q_{0\alpha i}(x)$, the differential operator $\widehat{L}_{ij}$ and the weight functions $\rho_{\alpha i}$ are fully determined by the second variational derivative $\frac{\delta^2 F}{\delta q_i \delta q_j}$. The condition $\delta^2\Phi > 0$ requires that all $\lambda_\alpha > 0$. The corresponding differential equations will be given below when the specific situations are be considered.

Equation (14) determines a set of the eigenvalues λ_α and the eigenfunctions $\delta q_{\alpha i}$ for the every solution $q_{0\alpha}$. Parameters λ_α and eigenfunctions $\delta q_{\alpha i}$ have a simple physical sense. The eigenfunctions $\delta q_{\alpha i}$ can be considered as amplitude functions of low energy spin waves or magnons. The eigenvalues λ_α are proportional to the square of magnon frequencies ω related to the $q_{0\alpha}$-magnetic structure, namely $\lambda_\alpha = \chi_\perp \omega_\alpha^2(k)/\gamma^2$, where k is the wave number of magnons, γ is the gyromagnetic ratio. In the following we will analyze the magnon frequencies $\omega_\alpha^2(k)$ rather than the eigenvalues λ_α.

For numerical calculations, we will also use the Cartesian representation of the antiferromagnetic vector $\boldsymbol{l} = (l_x,l_y,l_z)$. In this case Eq. (13) acquires the form

$$\frac{\delta F(\boldsymbol{l})}{\delta \boldsymbol{l}} = \lambda_0 \boldsymbol{l}_0, \tag{15}$$

where λ_0 is undetermined Lagrange multiplier. Equation (15) can be written as follows

$$\frac{\delta F(\boldsymbol{l}_0)}{\delta \boldsymbol{l}} \times \boldsymbol{l}_0 = 0 \tag{16}$$

In its turn Eq. (14) yields

$$\sum_{j=x,y,z}\left(\frac{\delta F(\boldsymbol{l})}{\delta l_i \delta l_j} - \lambda_0\delta_{ij}\right)\delta l_{j\alpha} = \lambda_\alpha \delta l_{i\alpha} \tag{17}$$

Note that conditions of transitions between magnetic phases q_α can be described in terms of (14). Eigenvalues λ_α change with the change of control parameters such as magnetic field or intrinsic magnetic anisotropy. In the case when the phase $q_{0\alpha}$ loses its stability the parameter λ_α changes its sign. In other words, one of numbers λ_α becomes equal to zero approaching to the critical point of phase transitions. In accordance with Landau theory this circumstance determines the soft mode of antiferromagnetic vector oscillations. The condition of the phase $q_{0\alpha}$ loss of stability is determined by the vanishing of minimal eigenvalues λ_α. Later on we consider phase diagrams of magnetoelectric antiferromagnet in terms of H and κ_c.

The intrinsic magnetic anisotropy of BFO multiferroics has a complicated character depending on the variations of temperature, doping of rare-earth ions, stresses arising during film growth, and lattice mismatch.[20,42–45,53,56–58] Magnetic anisotropy of BFO-like crystals is governed by several competing mechanisms including the single-ion anisotropy, anisotropic superexchange coupling, and magnetodipole interactions. In its turn the single-ion magnetic anisotropy can be divided into several contributions attributed to the symmetry of magnetic ions surrounding; the exchange coupling mechanism includes the antisymmetrical Dzyaloshinskii-Morya exchange along with other relativistic exchange contributions of quasidipolar and nondipolar types. An overall dependence of magnetic anisotropy of the crystal on internal and external parameters, e.g., concentration of rare earth ions and temperature variations, is determined by the corresponding behavior of its constituting components.[20,56]

In magnetic films magnitude and nature of the magnetic anisotropy may differ from those in a bulk crystal, which may lead to differences in the states of their spin subsystems. Magnetic anisotropy of the film depends on a number of factors: the effect of roughness, shape of a sample, dipole-dipolar interactions, etc.[59,60] One of the important mechanisms of change in the magnetic anisotropy of the films is the magnetostriction arising due to the presence of elastic stresses caused by the mismatch of the lattice parameters of the film and the substrate. In the case of (111)-oriented BFO films the magnetoelastic energy density attributed to magnetostriction effect can be written in the form

$$\begin{aligned} F_{m.\text{elas.}} = {} & B_1\left(l_x'^2 u_{xx}'^2 + l_y'^2 u_{yy}'^2 + l_z'^2 u_{zz}'^2\right) \\ & + B_2\left(l_x' l_y' u_{xy}' + l_x' l_z' u_{xz}' + l_y' l_z' u_{yz}'\right), \end{aligned} \tag{18}$$

where B_1, B_2 are the magnetoelastic coupling coefficients accessible from experimental determination[54,61] or *ab initio* calculations,[62] l_i' are the components of antiferromagnetic vector, u_{ik}' are the components of deformation tensor taken in the Cartesian coordinate frame $\boldsymbol{X}'$ related to crystallographic axes [100], [010], [001]. One can show that in the coordinate system $\boldsymbol{X}$ connected with the principal crystal axis $\boldsymbol{C}_3 \| \langle 111\rangle$ the magnetoelastic energy density given by (18) causes an additional contribution to the magnetic anisotropy of the form

$$F_{m.\text{elas.}} = -\frac{B_2 u_0}{2} l_z^2. \tag{19}$$

In view of the above consideration it is interesting to discuss the change of the ground state of the antiferromagnetic multiferroics by varying the energy of the magnetic anisotropy and exchange parameters. We treat BFO multiferroics placed in magnetic field applied along the principal crystal axis and in the perpendicular direction. In the latter case we investigate the influence of variation of the direction of magnetic field in the basal plane of a sample relative to the direction of space modulation of antiferromagnetic cycloid. Hereinafter we consider homogeneous magnetic states, incommensurate

structures, and related phase diagrams for each orientation of the magnetic field.

III. MAGNETIC FIELD $H \| OZ$ APPLIED PERPENDICULAR TO THE FILM PLANE

Let us consider the case $\boldsymbol{H} \| \boldsymbol{OZ}$ choosing Cartesian coordinate frame connected with the principal crystal axis $\boldsymbol{C}_3 \| \langle 111 \rangle : \boldsymbol{OX} \| [1\bar{1}0], \boldsymbol{OY} \| [11\bar{2}], \boldsymbol{OZ} \| [111]$.

A. Homogeneous magnetic states

In the case $\boldsymbol{H} \| \boldsymbol{OZ}$ the uniform part of the free energy density (12) is represented as

$$E_0 = \tfrac{1}{2}\left(\kappa_c + \kappa_m h^2\right) l_z^2 = -\tfrac{1}{2}\left(\kappa_c + \kappa_m h^2\right)\left(l_x^2 + l_y^2\right). \quad (20)$$

One can see that the magnetic field applied along the principal crystal axis renormalizes the constant of magnetocrystalline anisotropy. Dependent on a sign of effective anisotropy constant $\kappa_{\text{eff}} = \kappa_c + \kappa_m h^2$ a homogeneous magnetic state of the easy plane $|l_y| = 1$ or the easy axis $|l_z| = 1$ type is realized. As follows from (20) the phase $|l_z| = 1$ exists when $h > \sqrt{-\kappa_c/\kappa_m}$. The exchange and the nonuniform magnetoelectric interactions result in the appearance of inhomogeneous magnetic phases and the shift of boundaries of homogeneous phase transitions.

To analyze the stability of homogeneous state it is necessary to solve the eigenvalue problem and to find the spectrum of natural oscillation frequencies $\omega(\boldsymbol{k})$. For the definiteness we consider nonuniform perturbation of the homogeneous state $|l_y| = 1$. In accordance with (14) the stability condition defining natural frequencies of antiferromagnetic vector oscillations is determined by

$$(\omega^2 - k^2)(-\omega^2 + k^2 - (\kappa_c + \kappa_m h^2)) = 4k_x^2, \quad (21)$$

where $\boldsymbol{k}$ is the wave vector of spin waves, k_x is the x projection of vector $\boldsymbol{k}$ indicating the direction of spiral propagation.

Similar consideration can be applied for the analysis of the stability of any other easy plane state, in particular $|l_x| = 1$. However instability in the last case develops in $\boldsymbol{OY}$ direction.

Critical points of transition from homogeneous magnetic state into modulated structure associated with soft mode of oscillations (which is attained at zero values of minimum frequency) are determined from the dispersion equation (21). Equation (21) yields the saddle dependence of the smallest of natural frequencies' oscillation branches with two minimums in the k_x direction. The critical field of the transition into the homogeneous state is determined by the requirement of the vanishing of minimum frequency when the minimum is attained only at one (e.g., positive) value $k = k_x$. Following (21) one can define the critical field of the transition from the homogeneous magnetic state into the space-modulated structure.

$$h_c = \sqrt{\frac{4 - \kappa_c}{\kappa_m}}. \quad (22)$$

The curve representing dependence $\kappa_c(h)$ determined by (22) is shown on the phase diagram (Fig. 4) as line 3.

B. Incommensurate structures

To consider the structure and properties of inhomogeneous magnetic states we turn to the polar coordinate system with the polar axis aligned along the crystal principal axis and rewrite energy density (12) as

$$E = \frac{1}{2}[(\nabla\theta)^2 + \sin^2\theta\,(\nabla\varphi)^2] - \left[\cos\varphi\frac{\partial\theta}{\partial\widetilde{x}} + \sin\varphi\frac{\partial\theta}{\partial\widetilde{y}}\right] + \sin\theta\cos\theta\left(\sin\varphi\frac{\partial\varphi}{\partial\widetilde{x}} - \cos\varphi\frac{\partial\varphi}{\partial\widetilde{y}}\right) + \frac{1}{2}(\kappa_c + \kappa_m h^2)\cos^2\theta. \quad (23)$$

Corresponding Euler-Lagrange equations are

$$\Delta\theta + 2\sin^2\theta\left(\sin\varphi\frac{\partial\varphi}{\partial\widetilde{x}} - \cos\varphi\frac{\partial\varphi}{\partial\widetilde{y}}\right) + \sin\theta\cos\theta[(\kappa_c + \kappa_m h^2) - (\nabla\varphi)^2] = 0, \quad (24a)$$

$$\nabla(\sin^2\theta\nabla\varphi) + 2\sin^2\theta\left(\cos\varphi\frac{\partial\theta}{\partial\widetilde{y}} - \sin\varphi\frac{\partial\theta}{\partial\widetilde{x}}\right) = 0. \quad (24b)$$

In a general case the system of equations (24) allows a set of periodical solutions describing possible space modulated structures in multiferroics film. Periodical solutions differ from each other by space structure (magnetic configuration), areas of stability dependent on values of magnetic anisotropy constant, mismatch parameter, magnitude, and direction of applied magnetic field.

To consider conceivable periodical structures let us start from some simple approximations. In the case when magnetic anisotropy and magnetic field are absent, Eq. (24) has the solution $\theta_0 = k_x x + k_y y = (\boldsymbol{k}\cdot\boldsymbol{r})$, $\varphi = \arctan(k_y/k_x)$ describing harmonic cycloid. In the case when only the uniaxial magnetic anisotropy is taken into account the anharmonical solution of (24) described by elliptical functions is found as

$$\sin\theta = sn\left(\frac{\sqrt{\kappa_{\text{eff}}}}{\nu}\widetilde{x}; \nu\right), \quad (25)$$

where $sn(x;k)$ is the Jacobi elliptical function, $\kappa_{\text{eff}} = \kappa_c + \kappa_m h^2$, ν is the elliptical modulus $0 < \nu < 1$ determined from the minimum of averaged energy

$$\langle F\rangle = \frac{\kappa_{\text{eff}}}{\nu^2}\frac{E(\nu)}{K(\nu)} - \frac{\pi\sqrt{\kappa_{\text{eff}}}}{2\nu K(\nu)} - \frac{\kappa_{\text{eff}}}{2\nu^2},$$

where $K(\nu)$, $E(\nu)$ are complete elliptical integrals of the first and the second kind, φ is supposed to be constant. The other solution differing from (25) by the sign has not been considered since it is energetically disadvantageous. The theoretical analysis of the given above equations has been done for ferromagnet and antiferromagnet in works.[30,32]

A set of periodical solutions in magnetoelectric antiferromagnet belonging to the space symmetry group $R3c = C_{3V}^6$ has been considered in Ref. 34 dependent on the constant of uniaxial magnetic anisotropy. It has been shown therein that the new type of space-modulated structure, which is characterized by the conical distribution of antiferromagnetic vector arises along with the plane modulated structure. The first one is

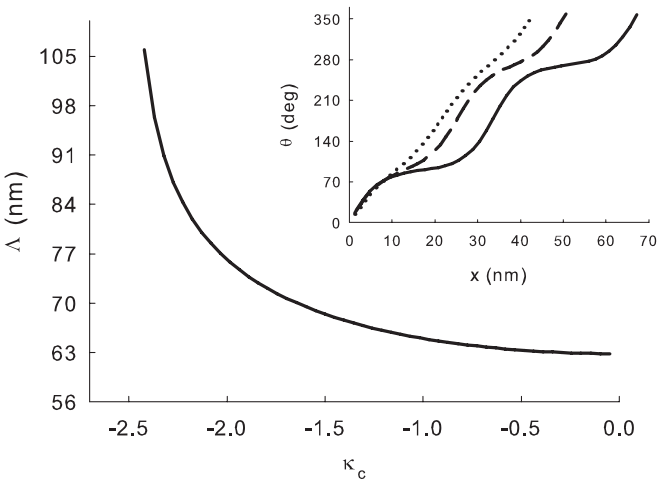

FIG. 2. Dependence of the period of Cy structure on the parameter κ_c. Inset: dependence $\theta(x)$. Solid curve corresponds to $\kappa_c = -2.4$, dashed curve corresponds to $\kappa_c = -2$, dotted curve corresponds to $\kappa_c = -1$.

denoted here as the cone cycloid CC state, which means that spins rotate a cone around the $\boldsymbol{OY}$ axis and the second one is denoted as the plane cycloid Cy state, which points out that $\boldsymbol{ZOX}$ is the plane of spin rotation. Besides that it should be noted that the plane modulated structure Cy slips into the CC phase in the case when hard plane anisotropy attains the critical value corresponding to $\kappa_{\text{crit1}} = 2.015$.

As was shown at the beginning magnetic field applied in the [111] direction renormalizes the constant of magnetic anisotropy so spin distribution in the cycloid in this case can be also described in a framework of Ref. 34 by taking into account the substitution $\kappa \to \kappa^h_{\text{eff}} = \kappa_c + \kappa_m h^2$. It is seen from Eq. (25) that the parameter ν defining spin arrangement in the cycloid can change in the interval $0 < \nu < 1$, which is accompanied with the subsequent change of the effective anisotropy constant $0 < \kappa^h_{\text{eff}} = \kappa_c + \kappa_m h^2 < \kappa_{\text{crit}}$. By taking into account the both relations one can find the critical field required for the destruction of space-modulated structure following the condition

$$h_c < \sqrt{\frac{\kappa_{\text{crit}} - \kappa_c}{\kappa_m}}.$$

The plot illustrating the dependence of the period of incommensurate structure $\Lambda = 4K(\nu)\nu/\sqrt{\kappa^h_{\text{eff}}}$ on the effective constant of magnetic anisotropy κ_c is represented in Fig. 2. It is seen that the spiral period changes with the varying of effective magnetic anisotropy. The period of spiral increases and tends to infinity at the critical value of κ_c corresponding to $\kappa_{\text{crit2}} = -2.467$. In this case the spiral state disappears, domain walls diverge to infinity, and the transition into the homogeneous easy axis state takes place. With κ_c decreasing the spiral length shrinks, but when κ_c changes its sign the spiral period increases again with the growth of modulus $|\kappa_c|$. When κ_c attains values corresponding to $\kappa_{\text{crit1}} = 2.015$ domains have no time to be formed and the commensurate structure transforms into conical state. With further change of effective magnetic anisotropy the cone converges to homogeneous easy

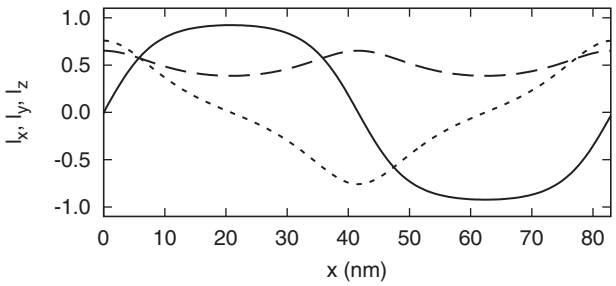

FIG. 3. Spin modulated structure, the scan of projections $\boldsymbol{l}(x) = (l_x(x), l_y(x), l_z(x))$ for the left symmetry CC solutions, solid line corresponds to the dependence $l_x(x)$, dashed line corresponds to the dependence $l_y(x)$, dotted line corresponds to the dependence $l_z(x)$, $H_z = 173$ kOe, $\kappa_c = 0.556$.

plane state at $\kappa_{\text{crit3}} = 4$ (see[34]). The scan of $\boldsymbol{l}$ projections in CC phase is shown in Fig. 3. As it is seen in Fig. 3 the antiferromagnetic vector goes out from the rotational plane in the CC phase.

C. Phase diagram $\boldsymbol{H \| C_3}$

The considered analysis together with the computer simulation allow us to reveal a set of magnetic phases realizing in multiferroics film in the magnetic field oriented in the [111] direction coinciding with the principal crystal axis $\boldsymbol{C}_3$. The obtained results are presented as the phase diagram or the map of incommensurate states stability shown in Fig. 4. The following four types of magnetic states are distinguished: homogeneous magnetic states of easy plane type $|l_y| = 1$ further on denoted as EP phase and easy axis type $|l_z| = 1$ denoted as EA phase, two types of incommensurate structures: the plane cycloid Cy and the conical cycloid CC being described by the corresponding solutions of the Euler-Lagrange

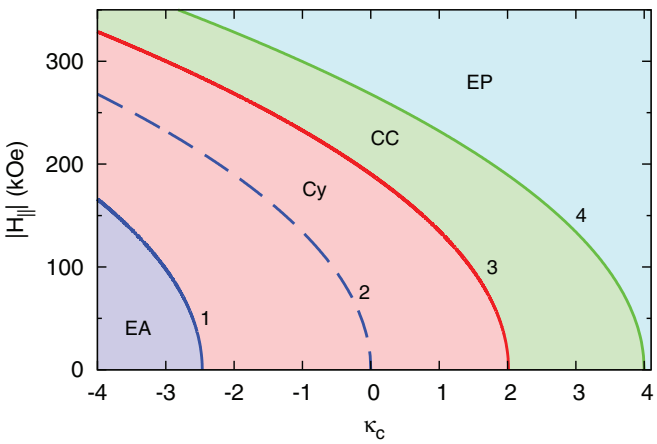

FIG. 4. (Color online) Phase diagram of a (111)-oriented BFO film, $\boldsymbol{H \| C_3}$. Line 1 corresponds to the transition from the plane cycloid Cy phase into the easy axis EA phase going over the phase domains growth, line 2 corresponds to the loss of EA phase stability, line 3 corresponds to the second-order phase transition between the Cy and the cone cycloid CC phases, line 4 corresponds to the second-order transition between CC and easy plane EP phases, the area restricted by lines 1, 2 is the metastable area of EA and Cy phases coexistence.

equations (24). The Cy solution corresponds to the cycloid developing in $\boldsymbol{ZOX}$ plane, the z and x components of antiferromagnetic vector of Cy phase are described by elliptical Jacobi functions, the y component of antiferromagnetic vector in this state is equal to zero. The plane of spin rotation in CC phase is different from the $\boldsymbol{ZOX}$ basal plane, all the components of antiferromagnetic vector of CC solution are different from zero. Magnetic states continuously transform into each other. The plane cycloid Cy continuously transforms into the conical cycloid CC with the right symmetry of spin rotation, the conical cycloid CC transforms into the easy plane $|l_y| = 1$ state when the magnitude of magnetic field and the magnetic anisotropy constant enhance. It should be noted here that the transition from the modulated Cy state into the homogeneous easy axis EA phase $|l_z| = 1$ goes over the nucleation of domain structure, the transition from plane-polarized Cy phase into the conical space-modulated structure CC and the transition into homogeneous easy plane state EP occur along the second-order transition line.

IV. MAGNETIC FIELD $\boldsymbol{H \| OX}$ APPLIED IN THE FILM PLANE

A. Homogeneous magnetic states

Consider the magnetic field applied in the $\boldsymbol{H \| OX} \| [1\bar{1}0]$ direction. We start from the determination of possible homogeneous magnetic phases, which can be found out from the uniform part of the free energy density

$$E_0 = \frac{1}{2}\kappa_c l_z^2 + \frac{1}{2}\kappa_m h^2 l_x^2 + \sqrt{\kappa_d \kappa_m} h l_y. \tag{26}$$

As follows from (26) the symmetrical phase $\boldsymbol{l} = (0, -1, 0)$ satisfies the minimum energy condition at positive values of $h_x > 0$ at $\kappa_c > -\sqrt{\kappa_d \kappa_m} h$. In the case $\kappa_c < -\sqrt{\kappa_d \kappa_m} h$ the tilted phase $\boldsymbol{l_0} = (0, -\sin\theta_0, \cos\theta_0)$, where $\sin\theta_0 = \sqrt{\kappa_d \kappa_m} h / |\kappa_c|$ possessing the energy $E = \kappa_d \kappa_m h^2 / 2\kappa_c$ arises. Therefore the transition between symmetrical and tilted phases occurs at $\kappa_c = -\sqrt{\kappa_d \kappa_m} h$ in the case when nonuniform contributions to the free energy are neglected.

To determine the boundary of the phase transition from the symmetrical easy plane phase $\boldsymbol{l}_0 = (0, -1, 0)$ into the space-modulated structure we refer to analysis of the stability of antiferromagnetic spin structure existing in the space uniform state by means of (14) resulting in the equation

$$(\omega^2 - h\sqrt{\kappa_d \kappa_m} - \kappa_c - k^2) \times (\omega^2 - h\sqrt{\kappa_d \kappa_m} - \kappa_m h^2 - k^2) = 4k_x^2 \tag{27}$$

allowing us to determine soft modes of spin excitations indicating to a possibility of phase transition. The soft mode of the transition corresponds to zero frequency of spin oscillations. As in the case considered in Sec. III A one can find that (27) yields the saddle dependence of the smallest of natural frequencies oscillation branches with two minimums in k_x direction. In the case of soft oscillation mode when the frequency tends to zero the following conditions are to be satisfied:

$$k_x^4 + k_x^2(\kappa_c + 2h\sqrt{\kappa_d \kappa_m} + \kappa_m h^2 - 4) + (\kappa_c + h\sqrt{\kappa_d \kappa_m})(\kappa_m h^2 + h\sqrt{\kappa_d \kappa_m}) = 0. \tag{28}$$

Here k_x is the x projection of magnon wave vector $\boldsymbol{k}$ indicating the direction of spiral propagation. The condition of merging two wave number values corresponds to the critical magnetic field value. Therefore the critical field of the transition from the homogeneous magnetic state into the space-modulated structure is defined as the minimum positive root of the equation

$$(\kappa_c + 2h\sqrt{\kappa_d \kappa_m} + \kappa_m h^2 - 4)^2 - 4(\kappa_c + h\sqrt{\kappa_d \kappa_m})(\kappa_m h^2 + h\sqrt{\kappa_d \kappa_m}) = 0. \tag{29}$$

Equation (29) determines the line of the transition from the symmetrical phase into the Cy-modulated structure corresponding to curve 1 on the phase diagram shown in Fig. 10.

The condition of the transition from the tilted magnetic phase into the incommensurate structure according to (14) is of the form

$$(\omega^2 - h\sqrt{\kappa_d \kappa_m}\sin\theta_0 + \kappa_c \cos 2\theta_0 - k^2) \times (\omega^2 - h\sqrt{\kappa_d \kappa_m}\sin\theta_0 + \kappa_c \cos^2\theta_0 - \kappa_m h^2 - k^2) = 4k_x^2 \sin^2\theta, \tag{30}$$

where θ_0 determines the polar angle of antiferromagnetic vector canting in the tilted phase. By taking into account that $\sin\theta_0 = -\sqrt{\kappa_d \kappa_m} h / \kappa_c$ when $0 < h < -\kappa_c / \sqrt{\kappa_d \kappa_m} h$ we reduce (30) to

$$\left(\omega^2 + \kappa_c - \frac{h^2 \kappa_d \kappa_m}{\kappa_c} - k^2\right) \times \left(\omega^2 + \kappa_c - \kappa_m h^2 - k^2\right) = 4k_x^2 \frac{h^2 \kappa_d \kappa_m}{\kappa_c^2}. \tag{31}$$

Proceeding in a similar way as in the previously considered case we find from (31) that the critical field of the transition is determined by the formula

$$h_c = -4\frac{\kappa_c / \sqrt{\kappa_m}}{\sqrt{2\kappa_c^2 + 8 + 8\kappa_c - \kappa_c \kappa_d - 16\kappa_d / \kappa_c - \kappa_c^3 / \kappa_d}}. \tag{32}$$

B. Incommensurate structures

The system of Euler-Lagrange equations determining possible incommensurate phases for the field $\boldsymbol{H \| OX}$ is written in the form

$$\Delta\theta + 2\sin^2\theta \left(\sin\varphi \frac{\partial\varphi}{\partial\tilde{x}} - \cos\varphi \frac{\partial\varphi}{\partial\tilde{y}}\right) + \sin\theta\cos\theta(\kappa_c - (\nabla\varphi)^2 - \kappa_m h^2 \cos^2\varphi) - \sqrt{\kappa_d \kappa_m} h \cos\theta \sin\varphi = 0, \tag{33a}$$

$$\nabla(\sin^2\theta \nabla\varphi) + 2\sin^2\theta \left(\cos\varphi \frac{\partial\theta}{\partial\tilde{y}} - \sin\varphi \frac{\partial\theta}{\partial\tilde{x}}\right) + \kappa_m h^2 \sin^2\theta \sin\varphi \cos\varphi - \sqrt{\kappa_d \kappa_m} h \sin\theta \cos\varphi = 0. \tag{33b}$$

In the absence of the magnetic field the only plane cycloid Cy state is realized. Numerical analysis of Eq. (33) shows that cone cycloids CC_+, CC_- differing by the direction of spin rotation appear when magnetic field is applied. For example

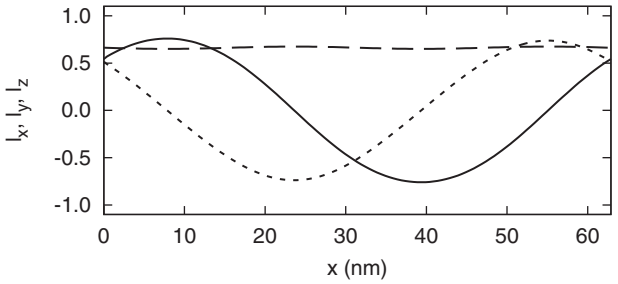

FIG. 5. Space distribution of the antiferromagnetic vector in the cone cycloid CC_+, solid line corresponds to the dependence $l_x(x)$, dashed line corresponds to the dependence $l_y(x)$, dotted line corresponds to the dependence $l_z(x)$, $H_x = -70$ kOe, $\kappa_c = 0.556$, $\kappa_d = 0.556$.

the spatial dependencies of vector $\boldsymbol{l}$ projections in the CC_+ state are presented in Fig. 5. The both CC_+ and CC_- states continuously arise from the Cy phase when the magnetic field is applied and continuously transform into the homogeneous easy plane EP state when the magnetic field grows as shown in Fig. 6.

As can be seen from plots in Fig. 6 and in the inset to this figure transitions between CC_+ and CC_- structures can be of the first and the second type, dependent on the value of the reduced anisotropy constant κ_c. In the area $\kappa_c < 2.015$ the transition between conical structures CC_+ and CC_- is of nonhysteretic character, in the area $\kappa_c > 2.015$ the transition between conical modulated structures becomes the first-order phase transition accompanied with hysteresis. Such change of the character of the phase transition can be caused as by the change in the uniaxial magnetic anisotropy in films and also by temperature variations of magnetic parameters in single crystals.

Due to the axial symmetry the space modulation in the spin subsystem can develop in any direction in the plane of the film in the absence of magnetic field. We have considered the

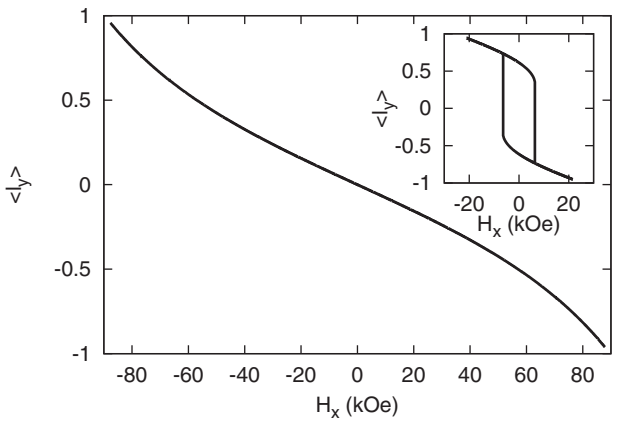

FIG. 6. The dependence of the space-averaged projection of the antiferromagnetic vector $< l_y >$ in the cone cycloid CC_+ on magnetic field starting from the initial plane cycloid Cy state, in the CC_+ state for the fixed value of $\kappa_c = 0.556$, $\kappa_d = 0.556$, $\kappa_m = 2.28 \times 10^{-5}$. Inset: the dependence of the space-averaged projection of the antiferromagnetic vector $< l_y >$ on the magnetic field calculated for $\kappa_c = 2.356$.

case when the magnetic field is applied along the direction of space modulation of antiferromagnetic structure. However the situation when the magnetic field is applied at an angle to the direction of space modulation is possible as well. Below we consider the limiting case corresponding to the magnetic field oriented in the direction transverse to the direction of space modulation.

V. MAGNETIC FIELD $\boldsymbol{H} \| \boldsymbol{OY}$ APPLIED IN THE FILM PLANE

Consider now magnetic phases and phase transitions in BFO film subjected to the magnetic field applied in the $\boldsymbol{H} \| \boldsymbol{OY} \| [11\bar{2}]$ direction.

A. Homogeneous magnetic states

As in the previous cases we begin with the exploration of homogeneous magnetic phases. The uniform part of the free energy density (12) acquires the form

$$E_0 = \tfrac{1}{2}\kappa_c l_z^2 + \tfrac{1}{2}\kappa_m h^2 l_y^2 - \sqrt{\kappa_d \kappa_m} h l_x. \tag{34}$$

We consider positive values of $h_y > 0$: in the case $\kappa_c > 0$ the minimum of the free energy density (34) corresponds to the symmetrical easy plane phase $\boldsymbol{l} = (1,0,0)$ (EP), in the case $\kappa_c < 0$ at $|\kappa_c| > \sqrt{\kappa_d \kappa_m}$ the tilted phase $\boldsymbol{l} = (\sin\theta_0, 0, \cos\theta_0)$, $\sin\theta_0 = \sqrt{\kappa_d \kappa_m} h / |\kappa_c|$ (T) arises.

The analysis of the stability of the symmetrical phase (EP) and the tilted phase (T) are quite similar to the case $\boldsymbol{H} \| \boldsymbol{OX}$ so for this situation we refer to Sec. IV A. The action of the magnetic field applied in $\boldsymbol{OX}$, $\boldsymbol{OY}$ directions in the basal plane due to the axial $\boldsymbol{C}_3$ symmetry should be equivalent, however the selected direction of the spiral propagation breaks the symmetry. In the case $\boldsymbol{H} \| \boldsymbol{OX}$ the plane cycloid Cy develops in $\boldsymbol{OX}$ direction, in the case $\boldsymbol{H} \| \boldsymbol{OY}$ the modulated in the plane $\boldsymbol{ZOY}$ Cy structure propagates in $\boldsymbol{OY}$ direction.

Thus we conclude that the critical magnetic field governing the stability of the symmetrical EP phase is determined by Eq. (29) deduced from the equation identical to (28), the transition from the T phase into the Cy structure is described by (32) following from the equation analogous to (31), in which k_x projections of the vector $\boldsymbol{k}$ are substituted by k_y projections.

B. Incommensurate structures

Turning next to inhomogeneous spin structures arising in the magnetic field $\boldsymbol{h} = (0, h_y, 0)$, we come back to the system of Euler-Lagrange equations, which in the considered case is represented in the form

$$\begin{aligned} &\Delta\theta + 2\sin^2\theta \left(\sin\varphi \frac{\partial \varphi}{\partial \tilde{x}} - \cos\varphi \frac{\partial \varphi}{\partial \tilde{y}} \right) \\ &\quad + \sin\theta\cos\theta(\kappa_c - (\nabla\varphi)^2 - \kappa_m h^2 \sin^2\varphi) \\ &\quad + \sqrt{\kappa_d \kappa_m} h \cos\theta \cos\varphi = 0, \end{aligned} \tag{35a}$$

$$\begin{aligned} &\nabla(\sin^2\theta \nabla\varphi) + 2\sin^2\theta \left(\cos\varphi \frac{\partial \theta}{\partial \tilde{y}} - \sin\varphi \frac{\partial \theta}{\partial \tilde{x}} \right) \\ &\quad - \kappa_m h^2 \sin^2\theta \sin\varphi \cos\varphi - \sqrt{\kappa_d \kappa_m} h \sin\theta \sin\varphi = 0. \end{aligned} \tag{35b}$$

Periodical solutions of (35) equations describe incommensurate spiral structures differing by magnetic configurations determined by spatial dependencies of θ,φ variables. Let us consider solutions with the determined plane of the rotation whose position is found at the following restriction

$$\frac{\partial\theta}{\partial\widetilde{y}} = 0, \tag{36a}$$

$$\sin\varphi = 0. \tag{36b}$$

Equation (36) implies spins to be rotated in the ZOX plane. The law of the spin distribution in the plane cycloid Cy is derived from the equation

$$\left(\frac{\partial\theta}{\partial\widetilde{x}}\right)^2 + \kappa_c \sin^2\theta + 2\sqrt{\kappa_d\kappa_m}h\sin\theta = c. \tag{37}$$

By integrating Eq. (37) one can obtain

$$\frac{\partial\theta}{\partial\widetilde{x}} = \pm\sqrt{c - \kappa_c\sin^2\theta - 2\sqrt{\kappa_d\kappa_m}h\sin\theta}, \tag{38}$$

which can be also represented as

$$\sin\theta = \frac{\gamma sn\left(\frac{\widetilde{x}}{a},\nu\right) + 1}{sn\left(\frac{\widetilde{x}}{a},\nu\right) + \gamma}, \tag{39}$$

where

$$a = \sqrt{\frac{\gamma^2 - 1}{c\gamma^2 - 2\sqrt{\kappa_d\kappa_m}h\gamma - \kappa_c}}$$

$$\nu = \sqrt{\frac{c - 2\gamma\sqrt{\kappa_m\kappa_d}h - \gamma^2\kappa_c}{c\gamma^2 - 2\gamma\sqrt{\kappa_m\kappa_d}h - \kappa_c}}$$

$$c\gamma = 2\sqrt{\kappa_d\kappa_m}h(\gamma^2+1) + 2\gamma\kappa_c.$$

The integration constant c is determined from the minimum condition of the Cy-phase energy

$$E = \frac{1}{2}\left(\frac{\partial\theta}{\partial\widetilde{x}}\right)^2 - \frac{\partial\theta}{\partial\widetilde{x}} - \frac{1}{2}\kappa_c\sin^2\theta - \sqrt{\kappa_d\kappa_m}h\sin\theta \tag{40}$$

averaged over a unit volume by use of (37)

$$\langle E\rangle = \frac{1}{\Lambda(c)}\int_0^{2\pi}\sqrt{c - \kappa_c\sin^2\theta - 2\sqrt{\kappa_d\kappa_m}h\sin\theta}d\theta - \frac{2\pi}{\Lambda(c)} - \frac{1}{2}c, \tag{41}$$

where

$$\Lambda = \int_0^{2\pi}\frac{d\theta}{\sqrt{c - \kappa_c\sin^2\theta - 2\sqrt{\kappa_d\kappa_m}h\sin\theta}} \tag{42}$$

is the spiral period.

We exclude the solution (38) with the negative sign since it is energetically disadvantageous. Minimization of the function (41) with respect to an unknown parameter c $d\langle E\rangle/dc = 0$ leads to the condition

$$\int_0^{2\pi}\sqrt{c - \kappa_c\sin^2\theta - 2\sqrt{\kappa_d\kappa_m}h\sin\theta}d\theta = 2\pi, \tag{43}$$

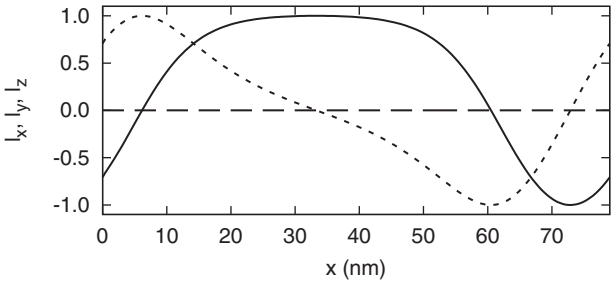

FIG. 7. Space distribution of antiferromagnetic vector in the Cy state, solid line corresponds to the dependence $l_x(x)$, dashed line corresponds to the dependence $l_y(x)$, dotted line corresponds to the dependence $l_z(x)$, $H_y = 70$ kOe, $\kappa_c = \kappa_d = 0.556$.

which allows us to calculate the averaged energy of Cy phase $\langle E\rangle = -c/2$. Formula (39) together with the condition (43) allows determining cycloidal structure. The scan of cycloid corresponding to $\kappa_c = 0.556$, $\kappa_d = 0.556$ at $H = 70$ kOe is represented in Fig. 7. The field dependence of the cycloid period calculated by the use of (42) for $\kappa_c = 0.556$ is shown in Fig. 8. It is seen that there is the critical field, the cycloid period increases without limit approaching to the critical field value. The unlimited growth of the period of cycloidal structure corresponds to the transition into space-homogeneous state.

One can estimate the critical points of the transition into homogeneous tilted and symmetrical phases $\kappa_c = \kappa_c(h)$ by comparing the energies of corresponding states. Let us restrict ourselves with negative values of uniaxial anisotropy constant since as was shown in Sec. IV A the tilted phase realizes in the area $|\kappa_c| > \sqrt{\kappa_d\kappa_m}h$, $\kappa_c < 0$, $d = \sqrt{\kappa_d\kappa_m}h$. As was shown in the very beginning in the case $d < -\kappa_c$ the tilted phase possessing with the energy $E = d^2/2\kappa_c$ is stable. It yields $c = -d^2/\kappa_c$ and the equation determining the critical line of transition is represented as follows:

$$\int_0^{2\pi}\sqrt{-\frac{d^2}{\kappa_c} - \kappa_c\sin^2\theta - 2d\sin\theta}d\theta = 2\pi. \tag{44}$$

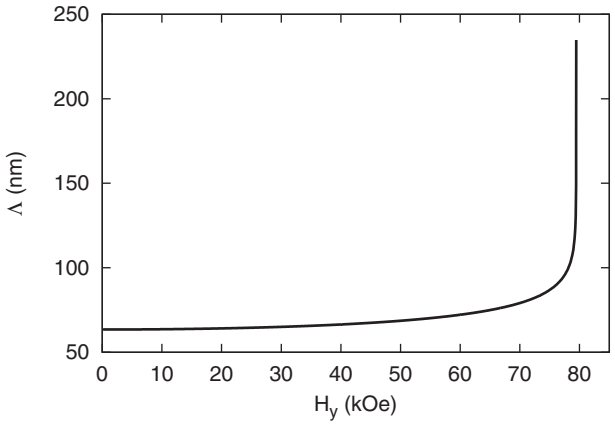

FIG. 8. Dependence of the period of CC state on magnetic field, $\kappa_c = 0.556$. The period increases with the growth of magnetic field tending to the infinity at the critical field corresponding to the transition into homogeneous easy plane state.

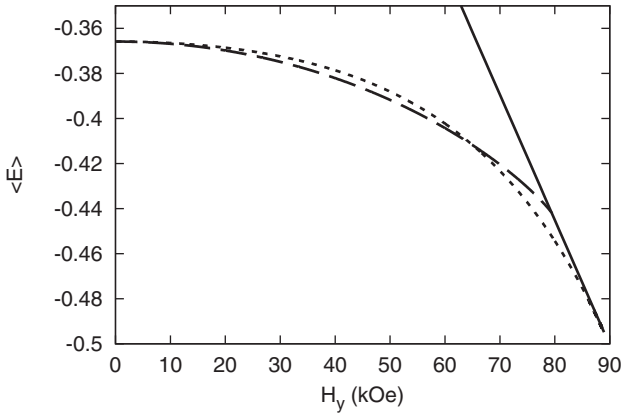

FIG. 9. Dependence of the average energy density of the structure on the magnetic field, solid line corresponds to the homogeneous EP phase, dashed line corresponds to the plane cycloid Cy, dotted line corresponds to the cone cycloid CC, $\kappa_c = 0.556$.

In the case $d > -\kappa_c$ the symmetrical phase $\theta = \pi/2$ possessing with the energy $E = -\kappa_c/2 - d$ occurs, $c = 2d + \kappa_c$ and the line of the transition from the Cy-modulated structure into the symmetrical phase is found as

$$\int_0^{2\pi} \sqrt{2d\,(1-\sin\theta) + \kappa_c(1-\sin^2\theta)}\,d\theta = 2\pi. \qquad (45)$$

However, the conditions of the transition of the considered plane cycloidal structure into homogeneous state are not physically meaningful. The homogeneous antiferromagnetic state can not be considered as the ground state on lines determined by (44), (45) where the period of cycloidal structure grows without limit. In the vicinity of these lines the ground state is represented by the space cycloid of conical type modulated along the direction of the applied magnetic field. In this connection we made numerical analysis of the plane and the cone cycloid energies dependent on the variations of magnetic field at the different values of reduced anisotropy parameter. The simulation shows that at low magnetic fields in the restricted range of anisotropy energy values the ground state corresponds to the plane cycloid modulated in the direction perpendicular to applied magnetic field. With magnetic field enhancement the energy of the cone cycloid modulated in the direction transverse to the direction of magnetic field approaches to the energy of the plane cycloid modulated along the magnetic field (Fig. 9). At the critical field value the energy of the plane cycloid becomes larger than the energy of the cone cycloid modulated in the direction perpendicular to the applied magnetic field. These values determine the line of the first-order phase transition, which is attained before reaching the critical values of magnetic field when the unlimited growth of the plane cycloid period occurs. The line of this transition is shown by lines 6, 7, 7' on the diagram Fig. 10.

C. Phase diagram $\boldsymbol{H \perp C_3}$

We summarize the results of the analysis of homogeneous and incommensurate magnetic phases for the considered antiferromagnetic system in BFO film with Hamiltonian (12) for the case of magnetic field applied perpendicular to the principal crystal axis $\boldsymbol{H \perp C_3}$.

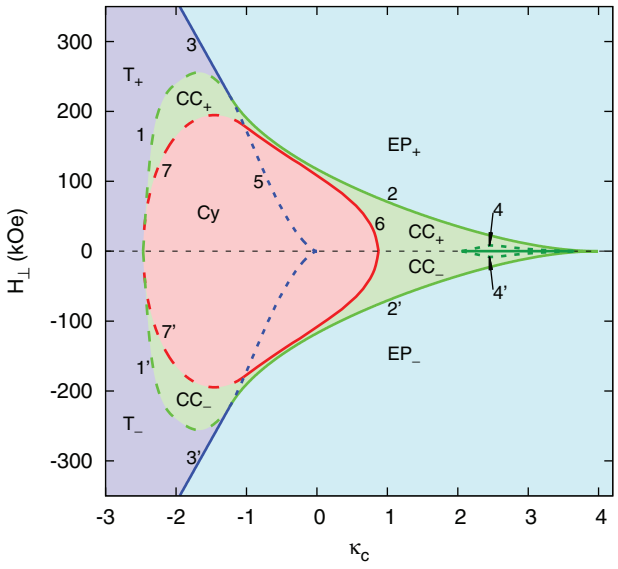

FIG. 10. (Color online) Phase diagram of a (111)-oriented BFO film, $\boldsymbol{H \perp C_3}$. Lines 1, 1' correspond to the transition from cone cycloids CC_+, CC_- into tilted phases T_+, T_-, lines 2, 2' restrict the area of homogeneous phases EP_+, EP_- stability, lines 3, 3' correspond to the second-order transition between easy plane states EP_+, EP_- and tilted phases T_+, T_-, lines 4, 4' are the lines of the loss of stability of cone cycloids CC_-, CC_+, line 5 corresponds to the line of the loss of stability of T_+ and T_- phases, lines 6, 7, 7' correspond to the first-order transition between Cy and CC_+, CC_- phases.

For the definiteness we consider the diagram corresponding to the magnetic field oriented along $\boldsymbol{OY} \| [11\bar{2}]$ axis, the similar analysis is relevant for the magnetic field oriented in the perpendicular direction $\boldsymbol{OX} \| [1\bar{1}0]$. The areas of the existence and the stability of possible homogeneous (tilted phases T_+, T_-, easy plane phases EP_+, EP_-) and incommensurate magnetic structures (plane cycloid Cy, conical cycloids CC_+, CC_-) are distinguished on the diagram. In the phase T_+ $l_y > 0$ and in the phase T_- $l_y < 0$. The phases EP_+ ($H > 0$) and EP_- ($H < 0$) have the oppositely directed antiferromagnetic vectors in the film plane perpendicular to magnetic field. The conical phases CC_+ and CC_- differ by the sign of antiferromagnetic vector projection on the perpendicular to cycloid modulation direction $\boldsymbol{OY}$. The area of the ground states T_+ and T_- existence is restricted by lines 1, 3 and 1', 3'. Lines 3, 3', and 5 are lines of the loss of stability of these ground states. Lines 2 and 3 as well as lines 2' and 3' are lines of the second-order phase transition between easy plane EP_+, EP_- phases and space-modulated structures of the cone type CC_+, CC_-. They restrict the areas of the stability of homogeneous symmetrical easy plane phases EP_+ and EP_-. Lines 6, 7, 7' are lines of the first-order phase transition between the plane cycloidal space-modulated structure Cy and cone cycloidal structures CC_+, CC_-. The direction of space modulation is perpendicular to the orientation of the applied magnetic field in the considered Cy structure and parallel to the magnetic field in CC_+, CC_- structures. In the area situated inside these lines the ground state of multiferroics corresponds to Cy structure, in the outside area the ground state corresponds to CC_+, CC_- structures. Lines 4 and 4' are lines of the loss of the stability of the cone cycloidal structure with the opposite projection of

antiferromagnetic vector on the film plane comparing to the ground space-modulated state. They restrict metastable areas of the corresponding phases when the magnetic field changes its sign. In the area restricted by these lines there is the line of the first-order phase transition delimiting CC_+ and CC_- phases, which begins and ends with the tricritical points of the first-order liquid-vapor-like transition.

It should be noted here that dashed lines 1, 1' and 7, 7' are of a qualitative character, which is attributed to the difficulties of their precise definition in framework of numerical analysis. On the lines 1, 1' unlimited growth of the period of space-modulated structure occurs. The transition from the cone cycloids CC_+, CC_- into the homogeneous phases T_+, T_- goes over the unlimited expansion of the tilted phase domain. In the vicinity of the first-order transition lines 6, 7, 7' the metastable areas of the plane cycloid Cy and the cone cycloids CC_+, CC_- exist, however to determine the boundaries of their existence an additional analysis is required.

VI. CONCLUSION

Our findings show that the structure and types of incommensurate phases in BFO-like multiferroics, the character of phase transitions, and the phase diagrams substantially depend on the external magnetic field and the magnetic anisotropy. We stress as well the role of the strain induced magnetic anisotropy. The primary sequence of phases: homogeneous magnetic state, incommensurate phase, domain structure is driven by the constant of magnetic anisotropy, which depends on a number of factors, such as temperature, rare-earth ion doping, and magnetostriction appearing as a result of the lattice mismatch between film and substrate.

It has been shown that cycloidal states in BFO multiferroics can be transformed into the transverse conical spiral structure under the action of uniaxial stresses, driving magnetic field or temperature variations. Phase diagrams or maps of magnetic phases determining the ground state of multiferroics have been constructed for the magnetic fields applied along the principle crystal axis and in the basal crystal plane. These diagrams can be used as practical tools to interpret experimental data, for strain engineering design of (111)-oriented BFO films with compressive [corresponds to the left part of the diagram ($\kappa_c < 0$)] and tensile [corresponds to the right part of the diagram ($\kappa_c > 0$)] deformations.

Another important aspect of the performed research is the consideration of the critical magnetic field of the transition into the homogeneous magnetic state. It is known that the magnetic field can suppress the cycloid but the required destruction value of the field is too high in bulk materials, which makes them difficult to use. We have shown that in epitaxial multiferroics films the destruction field can be lowered due to the magnetoelastic effect. In the case when magnetoelastic contribution is not sufficient the cycloid can be suppressed by the magnetic field whose critical value is lower than the one in bulk materials. The critical magnetic field depends on the direction of the applied magnetic field; the given results show that its value becomes lower in the case when the magnetic field is applied in the film plane. Our approach gives an opportunity to explain experimental observations of antiferromagnetic restructuring of the BFO films not only with a magnetic field, but also with an electric field and with the change of the temperature in a variable range.[40,41]

ACKNOWLEDGMENTS

This work is supported by the Russian Foundation for Basic Research, Grant No. 11-07-12031, and by the Ministry of Education and Science of Russian Federation (Grants No. 14.B37.21.1090 and No. 16.513.11.3149). We thank T. Archer, D. Sando, and A. P. Pyatakov for discussions.

*gzv@anrb.ru

[1] G. Catalan and J. Scott, Adv. Mater. **21**, 2463 (2009).
[2] L. Martin, Dalton Trans. **39**, 10813 (2010).
[3] M. Bibes, Nature Mater. **11**, 354 (2012).
[4] J. Scott, Nature Mater. **6**, 256 (2007).
[5] R. Ramesh and N. Spaldin, Nature Mater. **6**, 21 (2007).
[6] N. A. Spaldin, *Magnetic Materials: Fundamentals and Applications* (Cambridge University Press, Cambridge, 2010).
[7] A. Pyatakov and A. Zvezdin, Phys. Usp. **55**, 557 (2012).
[8] W. Kleemann and P. Borisov, in *Smart Materials for Energy, Communications and Security*, edited by I. A. Luk'yanchuk and D. Mezzane (Springer, Dordrecht, Netherlands, 2008).
[9] G. Smolenskii and I. Chupis, Sov. Phys. Usp. **25**, 475 (1982).
[10] J. Seidel, L. Martin, Q. He, Q. Zhan, Y. Chu, A. Rother, M. Hawkridge, P. Maksymovych, P. Yu, M. Gajek *et al.*, Nature Mater. **8**, 229 (2009).
[11] S. Yang, L. Martin, S. Byrnes, T. Conry, S. Basu, D. Paran, L. Reichertz, J. Ihlefeld, C. Adamo, A. Melville *et al.*, Appl. Phys. Lett. **95**, 062909 (2009).
[12] J. Allibe, S. Fusil, K. Bouzehouane, C. Daumont, D. Sando, E. Jacquet, C. Deranlot, M. Bibes, and A. Barthelemy, Nano Lett. **12**, 1141 (2012).
[13] J. Dho, X. Qi, H. Kim, J. MacManus-Driscoll, and M. Blamire, Adv. Mater. **18**, 1445 (2006).
[14] S. M. Wu, S. A. Cybart, D. Yi, J. M. Parker, R. Ramesh, and R. C. Dynes, Phys. Rev. Lett. **110**, 067202 (2013).
[15] V. Kruglyak, S. Demokritov, and D. Grundler, J. Phys. D **43**, 264001 (2010).
[16] P. Rovillain, R. de Sousa, Y. Gallais, A. Sacuto, M. Méasson, D. Colson, A. Forget, M. Bibes, A. Barthélémy, and M. Cazayous, Nature Mater. **9**, 975 (2010).
[17] C. Michel, J. Moreau, G. Achenbach, R. Gerson, and W. James, Solid State Commun. **7**, 701 (1969).
[18] J. Bucci, B. Robertson, and W. James, J. Appl. Crystallogr. **5**, 187 (1972).
[19] J. Teague, R. Gerson, and W. James, Solid State Commun. **8**, 1073 (1970).
[20] A. Kadomtseva, A. Zvezdin, Y. Popov, A. Pyatakov, and G. Vorobev, JETP Lett. **79**, 571 (2004).

[21] S. Kiselev, R. Ozerov, and G. Zhdanov, Sov. Phys. Dokl. **7**, 742 (1963).
[22] I. Sosnowska, T. Neumaier, and E. Steichele, J. Phys. C **15**, 4835 (1982).
[23] A. Zalesskii, A. Zvezdin, A. Frolov, and A. Bush, JETP Lett. **71**, 465 (2000).
[24] A. Zalessky, A. Frolov, T. Khimich, A. Bush, V. Pokatilov, and A. Zvezdin, Europhys. Lett. **50**, 547 (2007).
[25] R. Przeniosło, A. Palewicz, M. Regulski, I. Sosnowska, R. Ibberson, and K. Knight, J. Phys.: Condens. Matter **18**, 2069 (2006).
[26] I. Sosnowska and A. Zvezdin, J. Magn. Magn. Mater. **140**, 167 (1995).
[27] A. Zvezdin and A. Pyatakov, Europhys. Lett. **99**, 57003 (2012).
[28] Y. Tokura and S. Seki, Adv. Mater. **22**, 1554 (2010).
[29] Y. Tokunaga, S. Iguchi, T. Arima, and Y. Tokura, Phys. Rev. Lett. **101**, 097205 (2008).
[30] I. Dzyaloshinskii, Zh. Eksp. Teor. Fiz. **47**, 992 (1964).
[31] A. Zhdanov, A. Zvezdin, A. Pyatakov, T. Kosykh, and D. Viehland, Phys. Solid State **48**, 88 (2006).
[32] M. Tehranchi, N. Kubrakov, and A. Zvezdin, Ferroelectrics **204**, 181 (1997).
[33] A. Khalfina, M. Kharrasov, and M. Shamsutdinov, Phys. Solid State **43**, 1538 (2001).
[34] N. Kulagin, A. Popkov, and A. Zvezdin, Phys. Solid State **53**, 970 (2011).
[35] N. Kulagin, A. Popkov, A. Zvezdin, and S. Soloviov, Solid State Phenomena **190**, 285 (2012).
[36] G. Le Bras, D. Colson, A. Forget, N. Genand-Riondet, R. Tourbot, and P. Bonville, Phys. Rev. B **80**, 134417 (2009).
[37] P. Chen, Ö. Günaydin-Şen, W. J. Ren, Z. Qin, T. V. Brinzari, S. McGill, S.-W. Cheong, and J. L. Musfeldt, Phys. Rev. B **86**, 014407 (2012).
[38] G. Vorob'ev, A. Zvezdin, A. Kadomtseva, Y. Popov, V. Murashov, and Y. Chernenkov, Phys. Solid State **37**, 1329 (1995).
[39] Y. Popov, A. Zvezdin, G. Vorob'ev, A. Kadomtseva, V. Murashev, and D. Rakov, Pis' ma Zh Eksp Teor Fiz **57**, 65 (1993).
[40] M. Tokunaga, M. Azuma, and Y. Shimakawa, in *Journal of Physics: Conference Series*, Vol. 200 (IOP Publishing, Bristol, 2010), p. 012206.
[41] M. Tokunaga, Front. Phys. **7**, 386 (2012).
[42] W. Ratcliff II, D. Kan, W. Chen, S. Watson, S. Chi, R. Erwin, G. McIntyre, S. Capelli, and I. Takeuchi, Adv. Funct. Mater. **21**, 1567 (2011).
[43] J. Zhang, Y. Li, Y. Wang, Z. Liu, L. Chen, Y. Chu, F. Zavaliche, and R. Ramesh, J. Appl. Phys. **101**, 114105 (2007).
[44] X. Ke, P. P. Zhang, S. H. Baek, J. Zarestky, W. Tian, and C. B. Eom, Phys. Rev. B **82**, 134448 (2010).
[45] S. Lee, T. Choi, W. Ratcliff, R. Erwin, S. W. Cheong, and V. Kiryukhin, Phys. Rev. B **78**, 100101(R) (2008).
[46] D. Sando, A. Agbelele, D. Rahmedov, J. Liu, P. Rovillain, C. Toulouse, I. C. Infante, A. P. Pyatakov, S. Fusil, E. Jacquet, C. Carrétéro, C. Deranlot, S. Lisenkov, D. Wang, J-M. Le Breton, M. Cazayous, A. Sacuto, J. Juraszek, A. K. Zvezdin, L. Bellaiche, B. Dkhil, A. Barthélémy, and M. Bibes, Nat. Mater. (2013), doi:10.1038/nmat3629.
[47] F. Bai, J. Wang, M. Wuttig, J. Li, N. Wang, A. Pyatakov, A. Zvezdin, L. Cross, and D. Viehland, Appl. Phys. Lett. **86**, 032511 (2011).
[48] J. Speck and W. Pompe, J. Appl. Phys. **76**, 466 (1994).
[49] Z. Ban and S. Alpay, J. Appl. Phys. **91**, 9288 (2002).
[50] M. Ramazanoglu, I. W. Ratcliff, Y. J. Choi, S. Lee, S.-W. Cheong, and V. Kiryukhin, Phys. Rev. B **83**, 174434 (2011).
[51] Y.-j. Zhang, H.-g. Zhang, J.-h. Yin, H.-w. Zhang, J.-l. Chen, W.-q. Wang, and G.-h. Wu, J. Magn. Magn. Mater. **322**, 2251 (2010).
[52] B. Ruette, S. Zvyagin, A. F. Pyatakov, A. Bush, J. F. Li, V. I. Belotelov, A. K. Zvezdin, and D. Viehland, Phys. Rev. B **69**, 064114 (2004).
[53] Z. Gabbasova, M. Kuz'min, A. Zvezdin, I. Dubenko, V. Murashov, D. Rakov, and I. Krynetsky, Phys. Lett. A **158**, 491 (1991).
[54] A. Zvezdin, A. Kadomtseva, S. Krotov, A. Pyatakov, Y. Popov, and G. Vorobev, J. Magn. Magn. Mater. **300**, 224 (2006).
[55] A. Egoyan and A. Mukhin, Phys. Solid State **36**, 1715 (1994).
[56] J. Zhang, X. Lu, J. Zhou, H. Sun, J. Su, C. Ju, F. Huang, and J. Zhu, Appl. Phys. Lett. **100**, 242413 (2012).
[57] A. Zalesskii, A. Frolov, T. Khimich, and A. Bush, Phys. Solid State **45**, 141 (2003).
[58] N. Wang, J. Cheng, A. Pyatakov, A. K. Zvezdin, J. F. Li, L. E. Cross, and D. Viehland, Phys. Rev. B **72**, 104434 (2005).
[59] P. Bruno and J. Renard, Appl. Phys. A **49**, 499 (1989).
[60] C. Chappert and P. Bruno, J. Appl. Phys. **64**, 5736 (1988).
[61] S. Kim, H. Choi, K. No, and S. Shin, J. Phys. D **43**, 165001 (2010).
[62] J. C. Wojdeł and J. Íñiguez, Phys. Rev. Lett. **103**, 267205 (2009).